International Forum on Aeroelasticity and Structural Dynamics
IFASD 2024
17-21 June 2024, The Hague, The Netherlands

NONLINEAR ANALYSIS OF A FLEXIBLE HALF-WING MODEL TESTED IN A SUBSONIC WIND TUNNEL WITH CONTROL-SURFACE FREEPLAY AND PRELOADING

Breno Moura Castro[1], Wellington Luziano Paulo Junior[2], Douglas Domingues Bueno[2], Cleber Spode[2]

[1]Embraer, Technology Development Department
Av. Brig. Faria Lima, 2170 – 12.227-901 São José dos Campos, SP, Brazil
breno.castro@embraer.com.br

[2]Former Embraer, Technology Development Department
Av. Brig. Faria Lima, 2170 – 12.227-901 São José dos Campos, SP, Brazil
wellingtonlpaulo@gmail.com
douglas.bueno@unesp.br
cspode@gmail.com

Keywords: Freeplay, describing function, preloading, LCO, limit cycle oscillation, wind tunnel, flexible model, aeroelasticity

Abstract: Wind tunnel tests were conducted using a flexible, half-wing model with a control surface. The main purpose of these tests was to evaluate a methodology developed to accomplish nonlinear aeroelastic analyses. A flexible connection of the control surface was fitted with a freeplay mechanism to introduce nonlinear effects in the system.

An important feature of the experimental setup was that the model was installed in the horizontal position inside the test section. Therefore, the control surface was subjected to preloading due to the moment around the hinge line generated by its own weight. Limit cycle oscillations (LCO) were observed in the subsonic wind tunnel tests but only when the equilibrium position of the control surface, which depends on the tunnel flow velocity, was within the freeplay deadspace.

The treatment of preloading found in the literature (see Laurenson and Trn [1]), however, was not developed for such a condition. The condition in which the preloading formulation was developed in Ref. [1] assumed that the equilibrium occurs only outside the freeplay deadspace. Therefore, a special treatment for a preload equilibrium inside the freeplay deadspace was developed, for frequency-domain aeroelastic analyses, based on the same assumptions of Ref. [1], for the present conditions. The new approach needed a method for determining the equilibrium position of the control surface for a given wind tunnel flow condition (preload parameter).

The determination of the control surface equilibrium position demanded specific aerodynamic coefficients along with mass and inertia properties of the aeroelastic system. Aerodynamics were evaluated both by Vortex Lattice and Computational Fluid Dynamics (CFD) methods. The results of such equilibrium position calculations, then the preloading parameter, agreed well with experiments.

The predictions of the adapted methodology for the aeroelastic analysis of a nonlinear system with preload were consistent with the experimental LCO frequencies and amplitudes evaluated in the wind tunnel tests.

1 INTRODUCTION

The presence of freeplay in airplane control surfaces is inevitable due to tolerances in manufacturing the mechanisms for the actuation of those surfaces. It is also verified in connections between the surface and the actuator and between the actuator and its attachment to the primary structure of the wing. The presence of freeplay, like other nonlinearities, may induce the appearing of aeroelastic phenomena and aeroelastic responses commonly known as LCO (limit cycle oscillations).

LCO may occur and generate structural damage in the aircraft due to exceeding of loading limits or structural fatigue. Furthermore, even if there is no structural damage, these oscillations may induce discomfort to the crew and passengers and even generate difficulties to fly the aircraft, either by inducing involuntary movement in the pilot's body or by making it difficult to read flight instruments.

Therefore, it becomes imperative to study methodologies capable of predicting the occurrence of this nonlinear aeroelastic phenomenon, along with its characteristics in terms of amplitude and frequency in several ranges of flight velocities. The LCO amplitude becomes an important parameter in evaluating structural loadings and the frequency is relevant, for instance, in the evaluation of parameters associated with fatigue life.

A methodology for the prediction of occurrence and characteristics of LCO for aeroelastic systems with concentrated nonlinearities was developed and implemented at Embraer. And, aiming to verify the effectiveness of such methodology, a wind tunnel test was designed using a flexible model of a half-wing with a control surface. The connection of this control surface with the main surface of the wing had a mechanism to introduce freeplay in that connection. Figure 1 presents a view of the wind tunnel model used in the tests. The control surface is shown in blue.

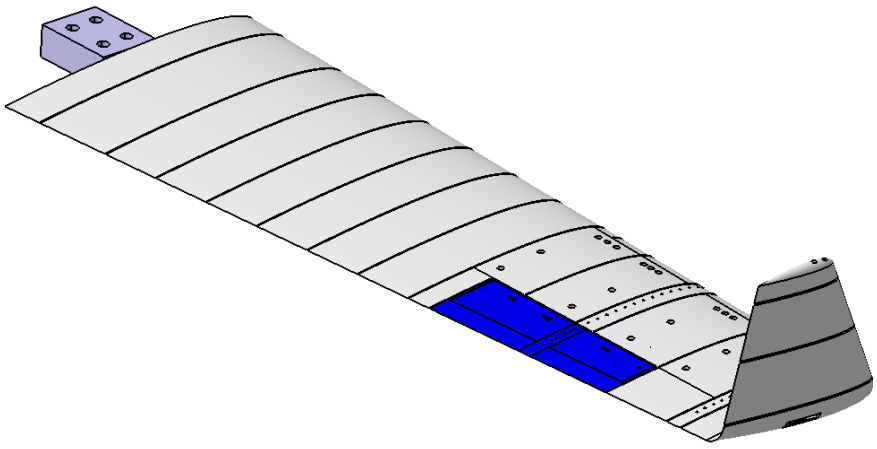

Figure 1: Isometric view of the flexible model used for the wind tunnel tests.

The flexible model used for the wind tunnel tests was designed by Embraer, using the implemented methodology, with the requirement to be able to generate LCO inside the operational envelope of the wind tunnel used for the tests. The chosen wind tunnel is a close-circuit and presents a test section of 3.00 x 2.10 m. Additionally, due to a control system that can adjust both the driving fan pitch and rotational velocity, the wind tunnel can generate flow velocities up to 120 m/s at the test section.

An important aspect of the present work refers to the installation of the flexible model in the test section of the tunnel. The first option for this type of installation typically is to place the model directly to the wind tunnel balance, used to measure the aerodynamic forces. This type of installation ends up with the model in a vertical position, exactly as the structure used to hold models for complete aircraft configurations. However, it was determined that the frequencies of the natural modes of vibration of the wind tunnel balance could interfere with the frequencies estimated for the aeroelastic phenomena to be observed. Then, an installation on the lateral wall of the wind tunnel test section was chosen. The consequence of such choice was the presence of preloading due to the action of gravity on the control surface.

Finally, the present work consists of simulations in the frequency domain, using the methodology implemented at Embraer, for the prediction of LCO characteristics and comparison with experimental data obtained in a wind tunnel. This comparison, ultimately, confirms the adequacy of the used methodology for the prediction of LCO occurrence in aircraft and its characteristics.

2 METHODOLOGY

The methodology used for the aeroelastic analysis of nonlinear problems involves two distinct approaches. The first one refers to the frequency domain and the second to the time domain. In this work, only analyses using the methodology in the frequency domain are conducted. Furthermore, experimental results obtained in the wind tunnel are used for comparison and verification of the methodology. Next sections of this text cover some theoretical concepts of the analysis in the frequency domain and some practical aspects of obtaining the experimental data necessary for the comparison with the theoretical methodology.

2.1 Frequency Domain Analysis

The frequency domain analysis is based on the Harmonic Balance Method. The book of Worden and Tomlinson [2] contains an excellent explanation of this method. The Harmonic Balance finds the best approximation of a nonlinear component of a dynamic system oscillating harmonically in a certain operating condition (characterized by an amplitude and frequency of oscillation) for an equivalent linear component as a function of the operational condition of the system. The equation describing the best linear approximation for this nonlinear component is known as the Describing Function [2].

However, due to the preloading condition mentioned earlier, the analysis to obtain the best linear approximation for the nonlinearity needs some adjustments. The equilibrium position of the system comes into the picture, as a consequence of the preloading force, in addition to the amplitude and frequency of oscillation. Therefore, the operating condition of the system consists of amplitude and frequency of oscillation and equilibrium position as a function of the preloading.

The work published by Laurenson and Trn [1] provides the treatment obtained by using the Harmonic Balance to a spring with a nonlinearity consisting of freeplay with preloading. When there is a dynamic system composed of a mass and a spring with freeplay and preloading, the equilibrium position occurs always in the region outside the deadspace or, in other words, in the region where the nonlinear spring presents stiffness and can generate an elastic force to neutralize the preloading force.

An excellent study and theoretical reference on the problem of freeplay with preloading is given by Verstraelen et al. [3]. This work demonstrated the existence of two-domain limit cycle

oscillations both theoretically and experimentally, besides given an outstanding theoretical basis for modeling and understanding this particular problem.

The situation inside the wind tunnel, when there is flow around the test model and this model is in the horizontal position, is such that the problem has an additional component to the ones considered by Laurenson and Trn [1]. The airflow can generate an aerodynamic force capable of counteracting the preloading force (gravitational) and makes it possible (even expected) to obtain conditions of equilibrium inside the freeplay deadspace. As far as this possibility was not treated by Laurenson and Trn and such study was not found in other references, there was a need to develop a treatment to an equilibrium condition inside the freeplay deadspace.

The approach by Laurenson e Trn is used as a reference to this work and it is presented initially. Next, the needed adaptations are discussed to obtain a mathematical formulation allowing the analysis of equilibrium conditions of the control surface inside the freeplay deadspace region.

The development of a Describing Function for the current problem is based on the schematic illustration shown in Fig. 2. The parameter P indicates the displacement of the equilibrium point due to the action of the preloading force, the variable δ translates the freeplay deadspace size, and the stiffness outside this region is represented by K.

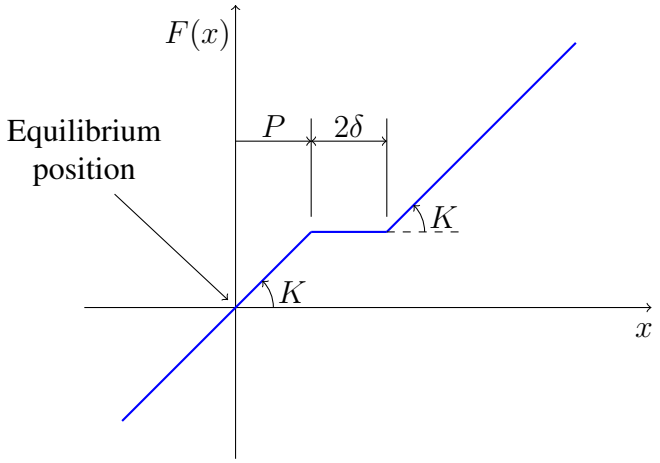

Figure 2: Model for the treatment of a nonlinearity of the freeplay with preloading type.

Treatment of problems involving preloading also differs from the normal approach to freeplay nonlinear problems by assuming that the average position of the response harmonic motion of the system is not the center of the freeplay zone or, in mathematical terms, the value of A_0 in Eq. (1) is not necessarily zero.

$$x(t) = A_0 + A_1 \cos \omega t \tag{1}$$

in which the coefficients A_0 and A_1 are defined as the average displacement and the amplitude, respectively, of the response motion of the system. These parameters can be determined, according to Laurenson and Trn, Ref. [1], using an assumption that the energy stored in the nonlinear spring is the same for both positive and negative displacements. This assumption leads to the relationships between A_0 and A_1 given by Eqs. (2) and (3).

$$A_1 = \frac{A}{2} + \frac{1}{2}\sqrt{2PA - P^2} \qquad \text{for } P < A \leq (P + 2\delta) \tag{2}$$

or

$$A_1 = \frac{A}{2} + \frac{1}{2}\sqrt{(A-2\delta)^2 + 4P\delta} \qquad \text{for } A > (P+2\delta) \tag{3}$$

where $A = A_0 + A_1$ and, according to the convention shown in Fig. 2, A_1 represents the amplitude of movement and A_0 translates the average displacement of the system with respect to the equilibrium position ($x = 0$).

It seems clear that, depending on the average position A_0 and the amplitude A_1, the movement of the system may not reach the freeplay region, only part of this region, or cover it entirely and reach the other side. In this last instance, both regions with stiffness contribute to the solution. For this reason, in case of preloading, there are more possibilities of Describing Functions in spite of only one involved in cases without preloading. The describing functions associated with preloading are:

$$\frac{K_{eq}}{K} = 1 \qquad \text{for } A \leq P \tag{4}$$

and

$$\frac{K_{eq}}{K} = \frac{1}{\pi}\left[\pi - \theta_1 + 2\left(\frac{P-A_0}{A_1}\right)\sin\theta_1 - \frac{1}{2}\sin 2\theta_1\right] \qquad \text{for } P < A \leq (P+2\delta) \tag{5}$$

in which:

$$\theta_1 = \arccos\left(\frac{P-A_0}{A_1}\right) \tag{6}$$

and

$$\begin{aligned}\frac{K_{eq}}{K} \;=\; & \frac{1}{\pi}\left[\pi + \theta_2 - \theta_1 - 2\left(\frac{P+2\delta-A_0}{A_1}\right)\sin\theta_2\right. \\ & \left. +2\left(\frac{P-A_0}{A_1}\right)\sin\theta_1 + \frac{1}{2}(\sin 2\theta_2 - \sin 2\theta_1)\right] \qquad \text{for } A > (P+2\delta)\end{aligned} \tag{7}$$

where

$$\theta_1 = \arccos\left(\frac{P+2\delta-A_0}{A_1}\right) \qquad \text{and} \qquad \theta_2 = \arccos\left(\frac{P-A_0}{A_1}\right) \tag{8}$$

These describing functions are suitable for cases in which the equilibrium position lies outside the freeplay deadspace region and will be referred to as *DF1* in this text.

Aiming to develop a model for cases where the equilibrium position is located inside that region, the convention depicted in Fig. 3, can be used.

The development of the equations for the case of equilibrium inside the freepaly region leads to:

$$\frac{K_{eq}}{K} = \frac{1}{\pi}\left[\theta_2 - \sin\theta_2\cos\theta_2 + \theta_1 - \sin\theta_1\cos\theta_1\right] \tag{9}$$

in which

$$\theta_1 = \arccos\left(\frac{P+2\delta-A_0}{A_1}\right) \qquad \text{and} \qquad \theta_2 = \arccos\left(\frac{A_0-P}{A_1}\right) \tag{10}$$

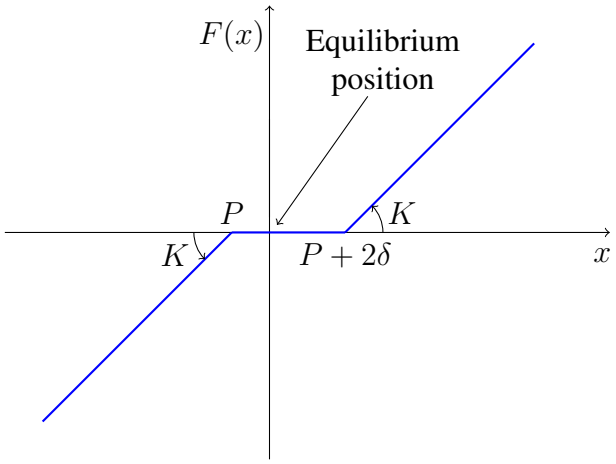

Figure 3: Model for studying freeplay with preloading and equilibrium position inside the deadspace region.

Equation (9) is in agreement with the equations developed in Ref. [3]. More specifically, Eq. (18) in page 16 can be easily related to the present describing function. The way to find a relationship between θ_1 and θ_2, however, is based on the work of Laurenson and Trn [1]. The assumption mentioned earlier, in which the same energy stored in the nonlinear spring occurs for both positive and negative displacements, brings about the following condition:

$$(\delta - A_1)(P - A_0 + \delta) = 0 \tag{11}$$

The satisfaction of Eq. (11), on its turn, imposes two different conditions:

(a) $\delta - A_1 = 0 \quad \Rightarrow A_1 = \delta$, resulting in a movement with amplitude exactly equal to the size of the freeplay deadspace.
(b) $P - A_0 + \delta = 0 \quad \Rightarrow A_0 = P + \delta$, representing a possible movement with $\cos\theta_1 = \delta/A_1$ and $\cos\theta_2 = \delta/A_1$.

Condition (a) implies $A_1 = \delta$ and this leads to a condition that $\cos\theta_1 = \cos\theta_2 = 1$ and, then, $A_0 = P + \delta$. This reflects a particular movement in which the control surface oscillates exactly inside the freeplay region, since $A_0 = P + \delta$, and then $K_{eq} = 0$. Therefore, this possibility of movement is discarded.

Concerning condition (b), one has to solve Eq. (9). This is a transcendental equation and needs a numerical procedure for finding its roots. It also needs the evaluation of $\arccos\theta_1$ and $\arccos\theta_2$. There are limitations of using this function to reach all possible solutions. For the present constraints, one can have only a small number of combinations for $\cos\theta_1$, $\sin\theta_1$, $\cos\theta_2$, and $\sin\theta_2$. To ease the implementation of a numerical procedure to find solutions of Eq. (9), one makes $\cos\theta_1 = \cos\theta_2 = \delta/A_1 = \xi$ and then:

$$\sin\theta_1 = \sqrt{1 - \xi^2} \qquad \text{and} \qquad \sin\theta_2 = \sqrt{1 - \xi^2}$$

Recalling that parameter A_0 can now be written as:

$$A_0 = P + \delta \tag{12}$$

and this mean position corresponds exactly to the center of the freeplay deadspace.

The Describing Function now becomes:

$$\frac{K_{\text{eq}}}{K} = \frac{2}{\pi}(\arccos\xi - \xi\sqrt{1-\xi^2}) \tag{13}$$

This describing function will be referred to as *DF2* and the associated equation for obtaining the solution for the amplitude of the movement is:

$$g(\xi) = \arccos\xi - \xi\sqrt{1-\xi^2} - \frac{\pi}{2}\left(\frac{K_{\text{eq}}}{K}\right) = 0$$

The equation that needs to be solved for the amplitude is transcendental and needs some numerical procedure. Newton-Raphson's technique is used in the present work for finding the root of transcendental equation ($g(\xi) = 0$) and it uses the following iterative process:

$$\xi^{(n+1)} = \xi^{(n)} - \frac{g(\xi^{(n)})}{g'(\xi^{(n)})}$$

The attempt to find small amplitude solutions, like the ones obtained in Laurenson and Trn [1] and represented by Eqs. 5 and 6, revealed that $\cos\theta_1 = 1$. This means there is no small amplitude motion satisfying the assumption that the same energy stored in the nonlinear spring occurs for both positive and negative displacements.

2.2 Equilibrium Position Evaluation

A parameter to be used in the analyses, when there is preloading in the aeroelastic system, is the equilibrium position where all forces are balanced. In the specific case of this test, the aerodynamic loading has an important contribution and, along with the gravitational force, determines the equilibrium position of the control surface.

Control surface equilibrium position can be determined, then, by means of a model of the wing's aerodynamics and the imposition of a zero resultant moment around the control surface hinge line. Aerodynamic moment around the hinge line is a function of both the angle of attack, α, and the control surface deflection angle, β, and it can be approximated by a first order Taylor series expansion around the point ($\alpha_0 = 0$, $\beta_0 = 0$):

$$C_H(\alpha,\beta) = C_{H_0} + C_{H_\alpha}\alpha + C_{H_\beta}\beta \tag{14}$$

where the parameter C_H represents the aerodynamic moment coefficient with respect to the hinge line (hinge moment) and C_{H_0}, C_{H_α}, and C_{H_β} are related to hinge moments for zero angle of attack and zero control surface deflection, the derivatives of the hinge moment coefficient with respect to the angle of attack and with the control surface deflection angle, respectively.

Evaluating the hinge moment aerodynamic coefficient:

$$H \approx \frac{1}{2}\rho V^2 S\, l(C_{H_0} + C_{H_\alpha}\alpha + C_{H_\beta}\beta) \tag{15}$$

where ρ is the air density, V translates the airflow velocity, S is the reference area and l represents the reference length used in the evaluation of C_H.

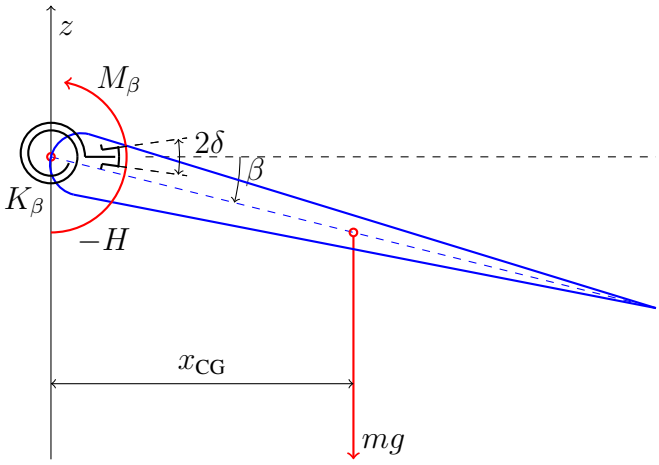

Figure 4: Schematic of forces and moments acting on the control surface.

The equilibrium position can be obtained by making the balance of moments around the hinge line, based on the schematic of Fig. 4:

$$M_\beta - H - mg\,x_{\text{CG}} = 0 \tag{16}$$

Doing the substitutions:

$$K_\beta(\beta_{\text{eq}} - \delta) - \frac{1}{2}\rho V^2 Sl(C_{H0} + C_{H\alpha}\alpha + C_{H\beta}\beta_{\text{eq}}) - mg\,x_{\text{CG}} = 0 \tag{17}$$

Solving Eq. (17) for β_{eq} and rearranging the terms, one ends up with:

$$\beta_{\text{eq}} = \frac{c + \delta - a(-C_{H0} - C_{H\alpha}\alpha)V^2}{1 - aC_{H\beta}V^2} \tag{18}$$

where:

$$a = \frac{\rho Sl}{2K_\beta} \qquad \text{and} \qquad c = \frac{mg\,x_{\text{CG}}}{K_\beta}$$

Equation (18) can be used for situations of equilibrium in which $\beta_{\text{eq}} < \delta_1$ or $\beta_{\text{eq}} > \delta_2$, according to the illustration in Fig. 5. Variable δ in Eq. (18) corresponds to δ_1 or δ_2 for $\beta_{\text{eq}} < \delta_1$ or $\beta_{\text{eq}} > \delta_2$, respectively.

In case the equilibrium position is in the region where $\delta_1 \leq \beta_{\text{eq}} \leq \delta_2$, there is no restoring moment in the spring due to freeplay. Then, the balance of moments around the hinge line can be rewritten as:

$$-H - mg\,x_{\text{CG}} = 0 \tag{19}$$

Substituting, simplifying, and rearranging terms, one obtains:

$$\beta_{\text{eq}} = \frac{c - a(-C_{H0} - C_{H\alpha}\alpha)V^2}{-aC_{H\beta}V^2} \tag{20}$$

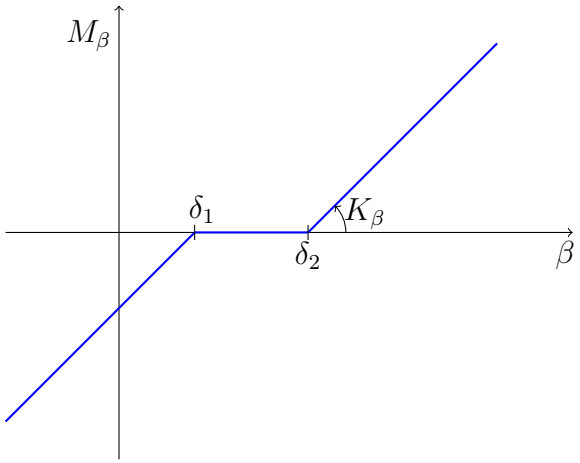

Figure 5: Model for the spring torque of the nonlinear rotational spring.

2.3 Test Data Reduction

Analysis of data obtained in the wind tunnel tests is based on the time history of control surface position. The test model was fitted with an RVDT (Rotary Variable Differential Transformer) mounted along the control surface hinge line to measure its angular position. Then, the reading of the RVDT transducer corresponds directly to the angular position of the control surface.

The transducer used in the tests is made by *Metrolog* and designated as RVDT RSYN-8-30. It can measure angles in range $-30^{\text{o}} \leq \beta \leq 30^{\text{o}}$, in an environment with vibrations up to $20g$, and in temperatures in the range $-55^{\text{o}}C \leq T \leq 105^{\text{o}}C$.

Transducer signal is analyzed using the Fourier transform to obtain the main oscillation frequency of the control surface. This frequency is relatively constant along the signal acquisition time and can be determined within an acceptable accuracy by taking a fragment of the measured signal for a certain test condition.

On the other hand, the oscillation amplitude presents a certain variation with time for a particular test condition. Therefore, a time window of the signal is selected and an average amplitude is calculated for this window. One must be careful to choose the signal window, striving to find a representative window for the evaluation of the LCO amplitude.

The additional parameter that appears in the preloading analyses is the control surface equilibrium position. This parameter can be experimentally obtained by computing the average in time, along the chosen time window, of the control surface position signal.

3 RESULTS

3.1 Control-surface Equilibrium Position

The evaluation of the aerodynamic moment around the control-surface hinge line was done by using the Vortex Lattice Method (VLM) of Drela [4]. The geometry discretization was done according to Fig. 6. A symmetry condition was used at $y = 0$ to simulate the boundary condition at the wind tunnel wall. 988 panels were used in the half-wing and 512 for the wind tunnel walls.

The modeling of the wind-tunnel test section was done by assuming that the walls are parallel to the x-axis and orthogonal to each other, forming a rectangular cross section with 2.1 m height and 3 m width. The length of the cross section was set to 4 m.

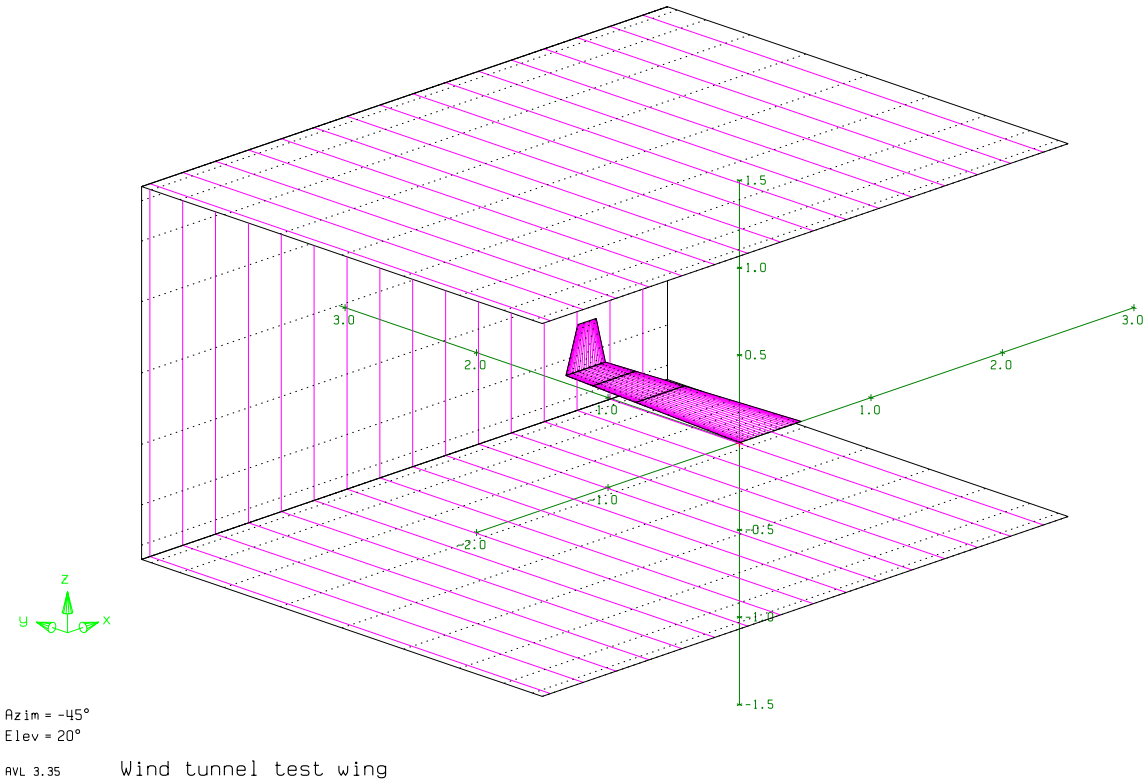

Figure 6: Discretization used for the half-wing and wind tunnel walls.

The half-wing itself was discretized with 26 horse-shoe vortices along the chord and 38 along the span, as it is illustrated in Fig. 7. This model was used, also, for the evaluation of the half-wing aerodynamics without the wind tunnel wall influence.

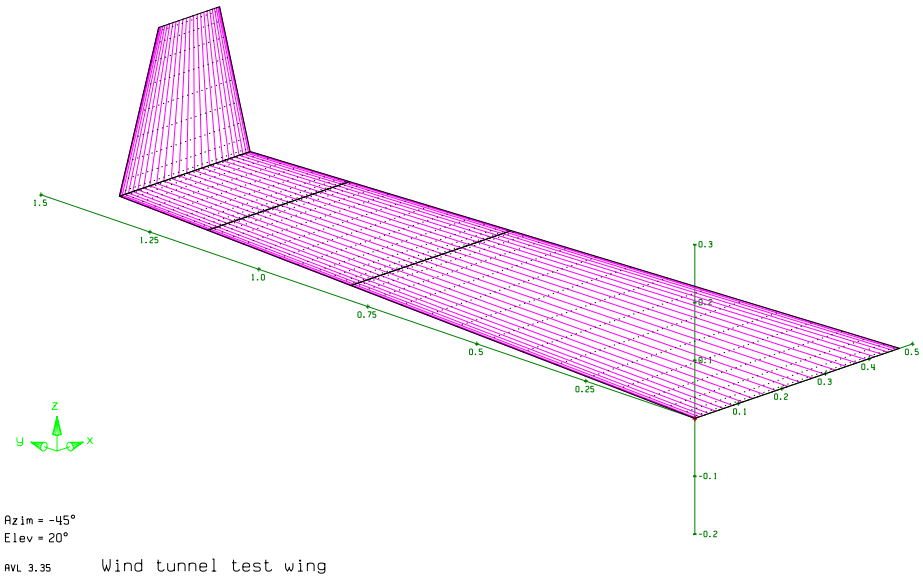

Figure 7: Details of the half-wing model discretization.

Tables 1 and 2 contain the results obtained for the lift (C_L) and moment coefficients around the control surface hinge line (C_H). Two discretizations of the half-wing were studied for convergency evaluation of the aerodynamic coefficients. It can be noticed that there is a small variation of the aerodynamic coefficient values, indicating that the convergency is acceptable.

Table 1: Simulations with wind tunnel walls for zero angle of attack.

$\alpha = 0$	$n_c = 24$ and $n_b = 30$ (half-wing) $n_c = 16$ and $n_b = 8$ (walls)		$n_c = 26$ and $n_b = 38$ (half-wing) $n_c = 16$ and $n_b = 8$ (walls)	
β (^{o})	C_L	C_H	C_L	C_H
-2	-0.02613	1.901×10^{-4}	-0.02622	1.898×10^{-4}
-1	-0.01307	9.504×10^{-5}	-0.01311	9.492×10^{-5}
0	0	0	0	0
1	0.01307	-9.506×10^{-5}	0.01312	-9.493×10^{-5}
2	0.02614	-1.901×10^{-4}	0.02623	-1.899×10^{-4}

Table 2: Simulations with wind tunnel walls for zero control-surface deflection.

$\beta = 0$	$n_c = 24$ and $n_b = 30$ (half-wing) $n_c = 16$ and $n_b = 8$ (walls)		$n_c = 26$ and $n_b = 38$ (half-wing) $n_c = 16$ and $n_b = 8$ (walls)	
α (^{o})	C_L	C_H	C_L	C_H
-2	-0.17864	1.522×10^{-4}	-0.17868	1.514×10^{-4}
-1	-0.08941	7.621×10^{-5}	-0.08943	7.580×10^{-5}
0	0	0	0	0
1	0.08955	-7.628×10^{-5}	0.08957	-7.587×10^{-5}
2	0.17919	-1.525×10^{-4}	0.17923	-1.517×10^{-4}

Additionally to the simulations with the inclusion of the wind tunnel walls in the mathematical model, calculations without the wind tunnel walls were performed, simulating a free-flow condition. Results of these computations are shown in Tabs. 3 and 4.

Table 3: Simulations without the wind tunnel walls for zero angle of attack.

$\alpha = 0$	Vortex Lattice Method $n_c = 26$ and $n_b = 38$ (half-wing)		CFD - Euler simulations
β (^{o})	C_L	C_H	C_H
-2	-0.02532	1.889×10^{-4}	1.430×10^{-4}
-1	-0.01266	9.447×10^{-5}	6.113×10^{-5}
0	0	0	-2.000×10^{-5}
1	0.01266	-9.448×10^{-5}	-1.011×10^{-4}
2	0.02533	-1.890×10^{-4}	-1.842×10^{-4}

Table 4: Simulations without the wind tunnel walls for zero control-surface deflection.

$\beta = 0$	Vortex Lattice Method $n_c = 26$ and $n_b = 38$ (half-wing)		CFD - Euler simulations
α (^{o})	C_L	C_H	C_H
-2	-0.17148	1.446×10^{-4}	9.535×10^{-5}
-1	-0.08583	7.240×10^{-5}	3.777×10^{-5}
0	0	0	-2.000×10^{-5}
1	0.08596	-7.247×10^{-5}	-7.820×10^{-5}
2	0.17199	-1.449×10^{-4}	-1.370×10^{-4}

For simulations without the wind tunnel walls, only computations with the finer discretization of the half-wing were carried out, since, for the previous case, there was no significant difference from the studied discretizations. Figures 8 and 9 show the aerodynamic loadings given by the Vortex Lattice Method.

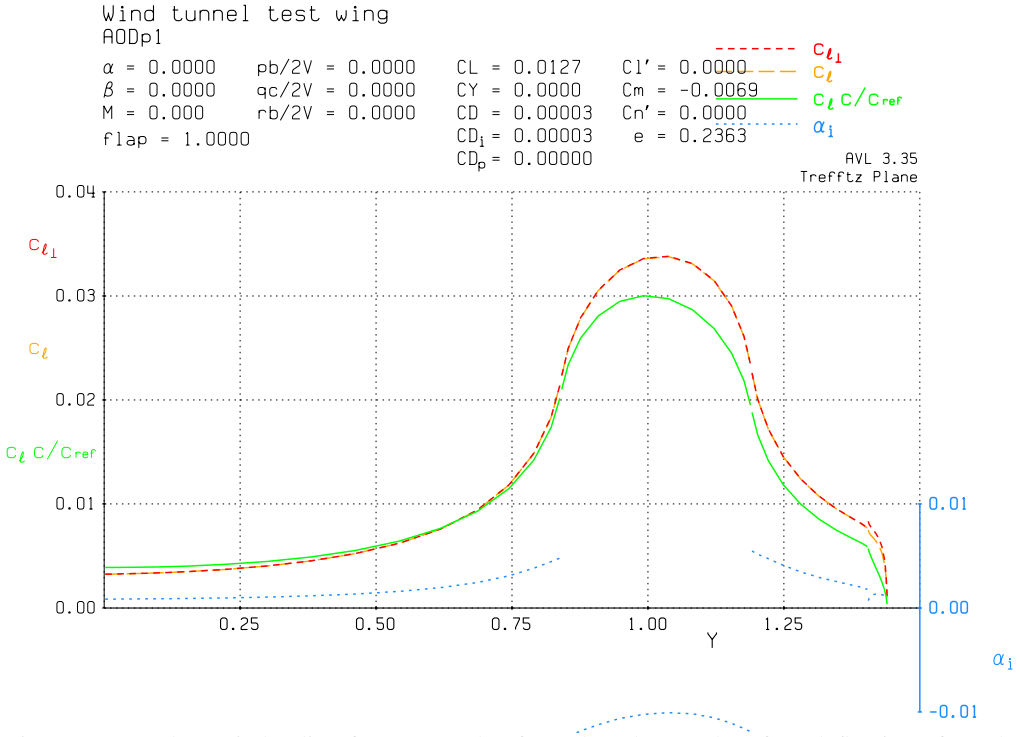

Figure 8: Aerodynamic loading for zero angle of attack and control surface deflection of 1.0 deg.

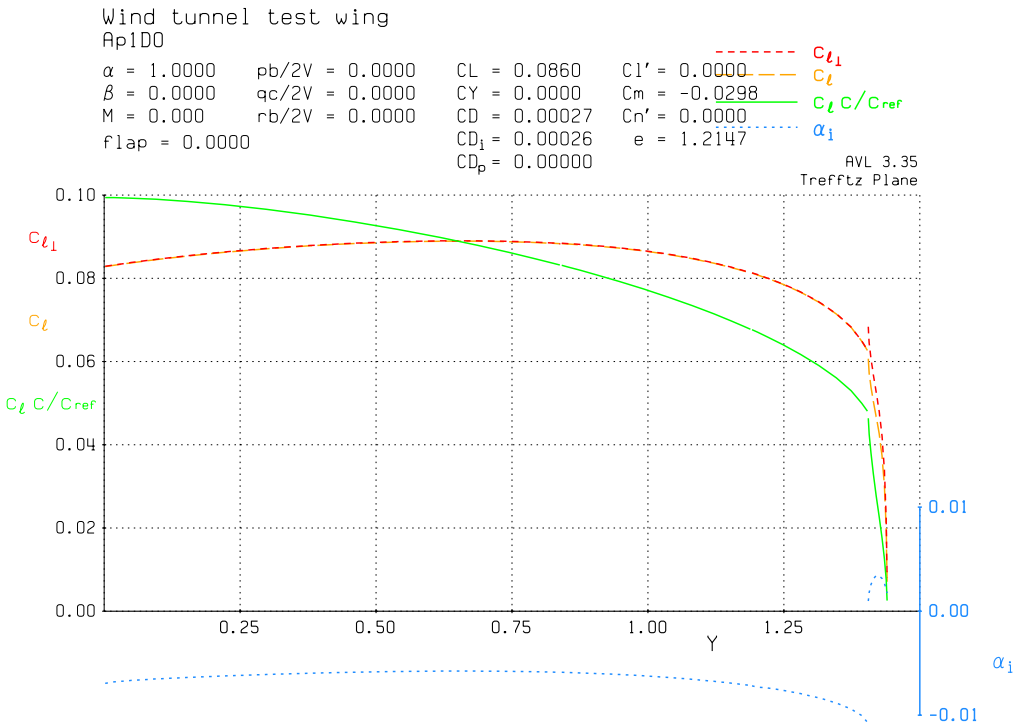

Figure 9: Aerodynamic loading for zero control surface deflection and 1.0 deg angle of attack.

One notices that the aerodynamic loading due to the control surface deflection only is concentrated in the control surface region (Fig. 8) and the aerodynamic loading due to the angle of

attack only (presented in Fig. 9) is distributed along the span (green line) as expected. For the cases including the wind tunnel walls, the observed behavior was identical.

The influence of the wind tunnel walls can be observed in Figs. 10 and 11. These figures also show the results obtained from a CFD code in which an Euler formulation (without viscous effects) was used. One important difference between analyses with VLM and CFD is that the wing profile thickness is considered only in the latter.

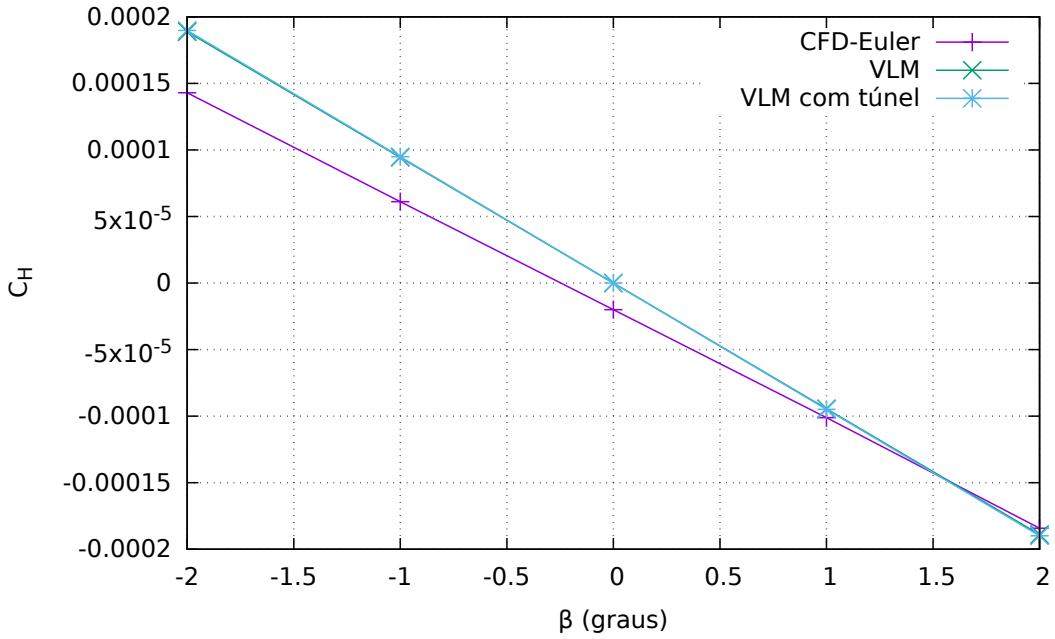

Figure 10: Moment coefficient variation with control surface deflection.

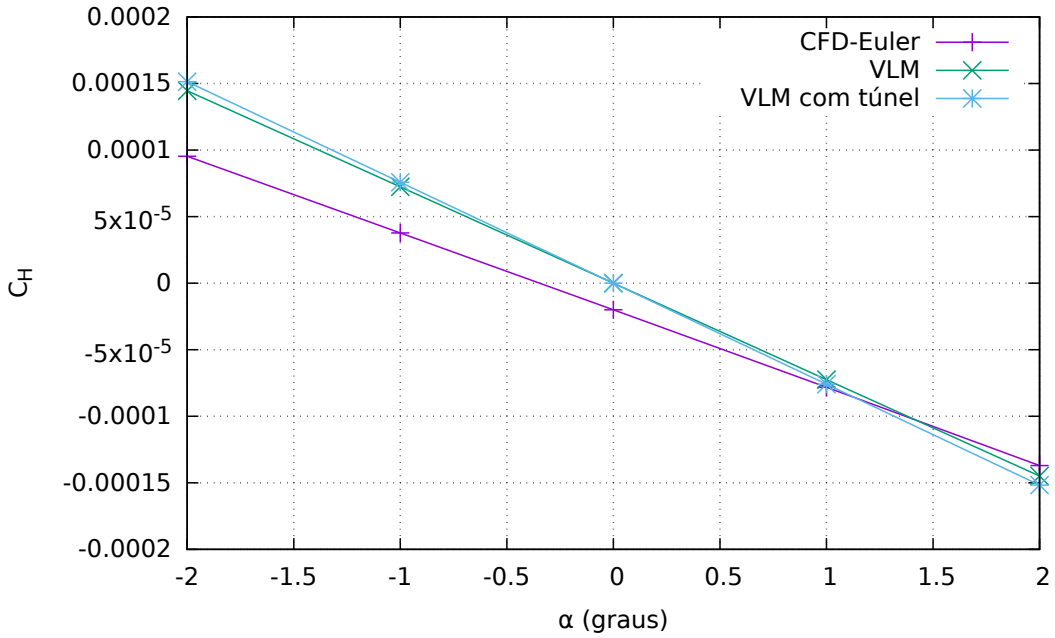

Figure 11: Moment coefficient variation with angle of attack.

Doing the computation of the aerodynamic hinge moment coefficient derivatives, one ends up with the data presented in Tab. 5.

Table 5: Results for the computation of control-surface aerodynamic hing-moment coefficient derivatives.

Method	C_{H0}	$C_{H\alpha}$	$C_{H\beta}$
VLM (half-wing)	0	-4.147$\times 10^{-3}$	-5.413$\times 10^{-3}$
VLM (half-wing + tunnel)	0	-4.365$\times 10^{-3}$	-5.446$\times 10^{-3}$
CFD-Euler (half-wing)	-2.00$\times 10^{-5}$	-3.328$\times 10^{-3}$	-4.686$\times 10^{-3}$

Some comments regarding the coefficients shown in Tab. 5 are relevant. All of them are estimated assuming a geometry perfectly symmetric for profiles of the half-wing sections. In reality, the profile geometries present some manufacturing distortions and imperfections. Even the wind tunnel flow in the wind-tunnel test section may present asymmetries and distortions as, for instance, an uneven velocity distribution. However, the only coefficient actually sensitive to these imperfections is C_{H0}. Therefore, it becomes quite unreasonable to use the value estimated for the C_{H0} coefficient.

On the other hand, the use of the Euler methodology in the computations, with a better level of fidelity to the wing profile geometry, revealed an important difference in derivatives $C_{H\alpha}$ and $C_{H\beta}$ with respect to the ones obtained with VLM. Wind tunnel walls, on their turn, did not have a significant influence in the aerodynamic moment coefficient derivatives.

The tested wind tunnel model (half-wing) has the parameters presented in Table 6.

Table 6: Data related to the tested wind tunnel model.

Parameter	Value
S	1.08185 m^2
l	0.39126 m
ρ	1.1 kg/m^3
g	9.81 m/s^2
m	1.3455 kg
x_{CG}	0.0253 m
δ_1	-1.715^o = -0.02993 rad
δ_2	1.715^o = 0.02993 rad
K_β	6.125 N.m/rad

The size of control-surface freeplay was measured following an Embraer internal procedure and the corresponding report is the one described in Ref. [5]. Figure 12 contains the measurement result.

Applying the values presented in Tab. 6 in the various equations discussed in this text, one obtains:

$$a = \frac{\rho S l}{2K_\beta} = 0.038018 \text{ s}^2/\text{m}^2 \qquad c = \frac{mgx_{\text{CG}}}{K_\beta} = 0.054534 \text{ rad}$$

Case $\delta_2 < \beta_{eq}$

$$\beta_{\text{eq}} = \frac{c + \delta_2 - a(-C_{H0} - C_{H\alpha}\alpha)V^2}{1 - aC_{H\beta}V^2} = \frac{0.084466 - 0.038018(-C_{H0} + 0.003328\alpha)V^2}{1 + 0.00017815\ V^2}$$

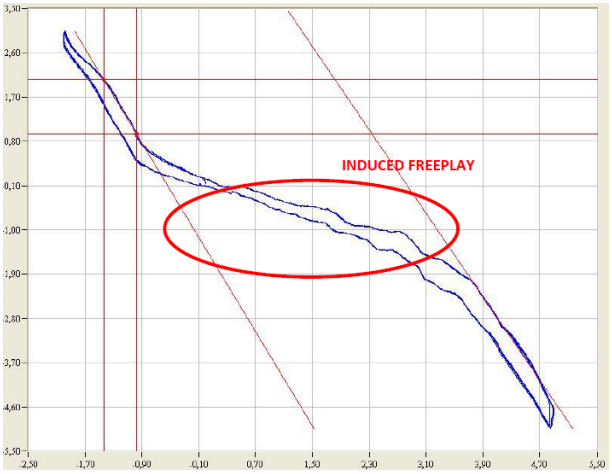

Figure 12: Force against displacement graph related to the control-surface freeplay measurement.

Case $\delta_1 \leq \beta_{eq} \leq \delta_2$

$$\beta_{\text{eq}} = \frac{c - a(-C_{H0} - C_{H\alpha}\alpha)V^2}{-aC_{H\beta}V^2} = \frac{0.054534 - 0.038018(-C_{H0} + 0.003328\alpha)V^2}{0.00017815\ V^2}$$

One notices that C_{H0} has a significant influence in the equilibrium position of the control surface. However, this coefficient is reasonably difficult to evaluate since it is highly affected by manufacturing imperfections in the model (assymmetries) and wind tunnel test section irregularities, as mentioned previously.

Considering this difficulty to estimate C_{H0} with some degree of accuracy and the observation that it has a significant influence on the control-surface equilibrium position, a value of $C_{H0} = -0.0002$ was chosen since it better correlates the numerically computed equilibrium position with the one observed experimentally.

3.2 Analysis of LCO characteristics - Frequency Domain

The mathematical model used to evaluate the unsteady aerodynamics, based on the Doublet Lattice Method (DLM), is shown in Fig. 13. The flow conditions, in this case, are subsonic and no adjustment or correction to the coefficients estimated by DLM was used. During the tests, all foreseeable measures were taken (besides constant monitoring) to avoid any other type of nonlinearity, such as flow detachments, to arise and interfere with the eventual LCO characteristics.

The finite element model created to estimate the structural dynamics behavior of the wind tunnel model is represented in Fig. 14. The elements used are basically beams with an specified stiffness and point masses placed at appropriate positions to represent a spatial mass distribution.

The equilibrium positions calculated with the previously presented methodology are shown in Fig. 16. Results measured in the wind tunnel are marked with black diamonds and data obtained with the present methodology are represented by blue circles.

One can verify that, when comparing theoretical data with the ones obtained with the methodologies here described, theoretical methods are able to estimate well the equilibrium position of the control surface subjected to gravitational force and freeplay.

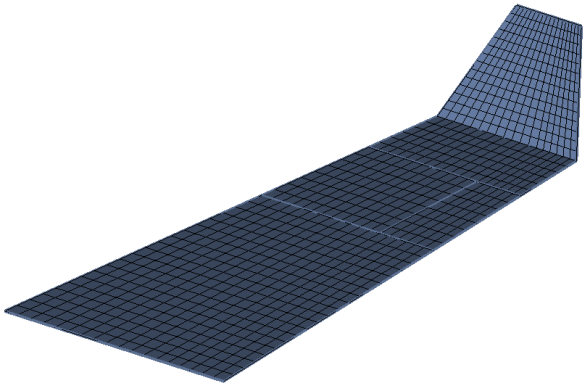

Figure 13: Half-wing geometry discretization used for the Doublet Lattice Method.

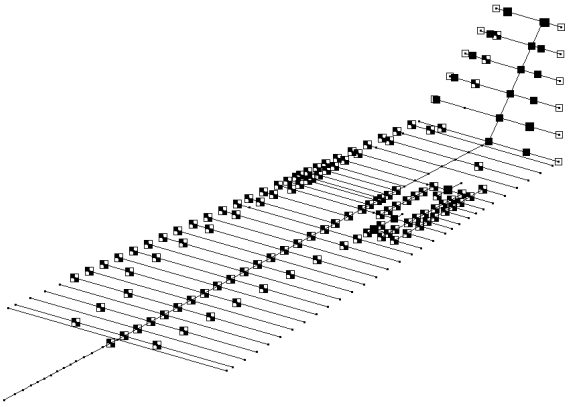

Figure 14: Schematic of the finite element model used for the Structural Dynamics.

An example of the time history of the control-surface position during the wind tunnel tests is given in Fig. 15. One clearly notices an oscillation of the control surface around an equilibrium position. Time histories, for various test conditions, were treated with Fourier analysis to obtain LCO amplitude and frequency.

Charts with LCO amplitudes and frequencies are illustrated in Figs. 17 and 18, respectively. They present LCO amplitudes and frequencies estimated with the frequency domain approach, represented by orange circles for DF1, by blue circles for DF2, and the values estimated from the data measured in the wind tunnel tests shown in black diamonds. The equations used for the estimation were the ones described in Section 2.1. The describing function, Eq. (13), obtained for the preloading condition gives approximately the same results as Den Hartog's equation, already widely validated for estimating LCO amplitudes without preloading.

In a preliminary manner, one notices that the predictions of LCO characteristics obtained with the describing function for the preload condition give results which are compatible with those obtained in the wind tunnel tests using a flexible model and fitted with a control surface with freeplay. All estimated experimental values are close but lower than the ones predicted with the describing function. This could be attributed to a number of factors as, for instance, the presence of some friction in the freeplay mechanism and some structural damping in the aeroelastic system.

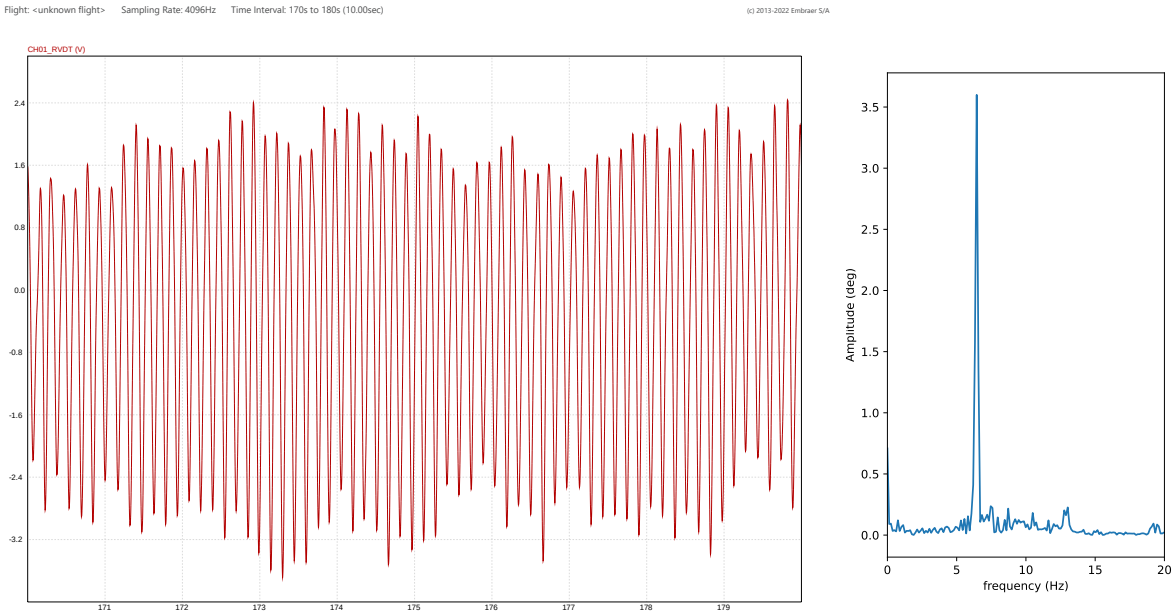

Figure 15: Control surface position variation measured and DFT analysis for $V = 90$ m/s.

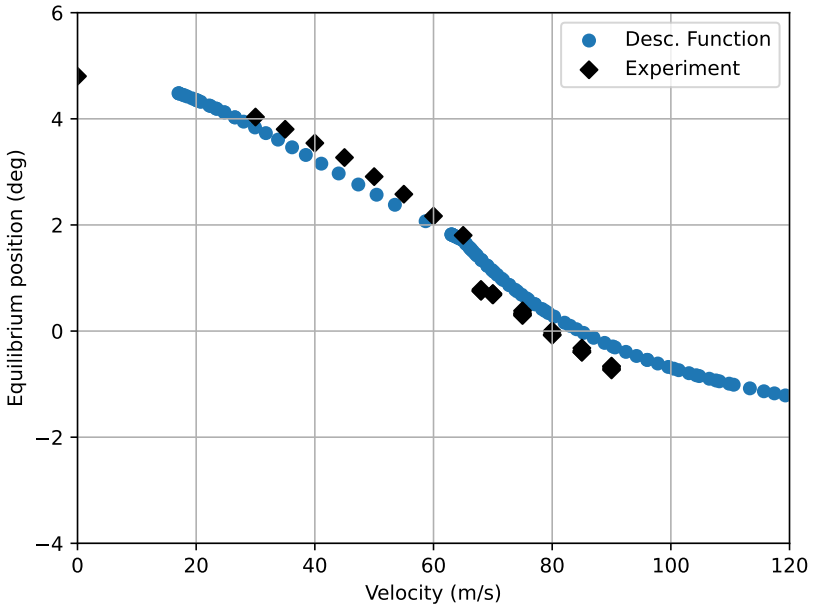

Figure 16: Comparison of control-surface average positions computed and measured.

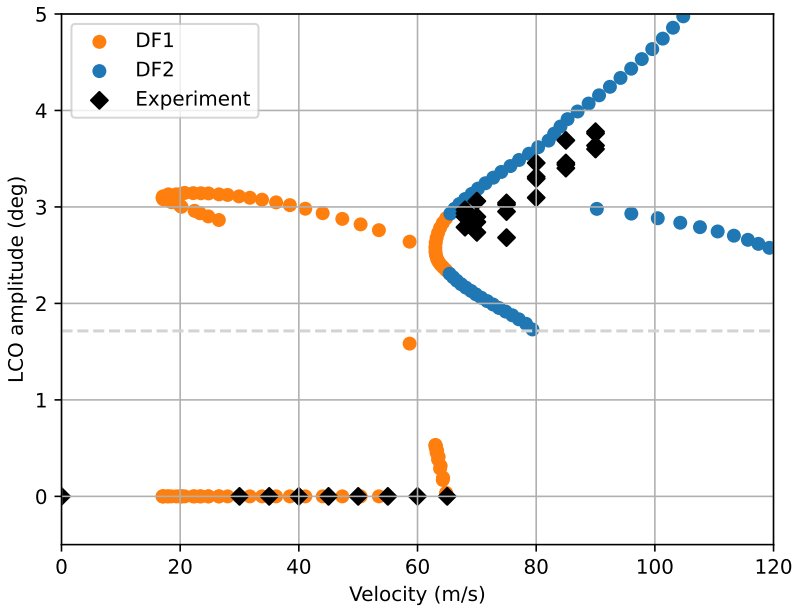

Figure 17: Comparison of LCO amplitudes estimated and measured.

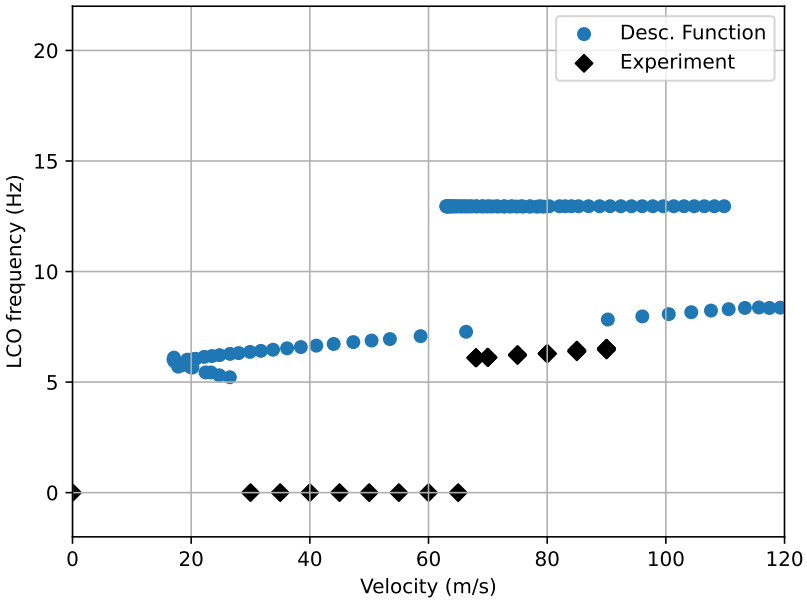

Figure 18: Comparison of LCO frequencies estimated and measured.

4 COMMENTS AND CONCLUSIONS

This work contains the methodology developed and used to predict and analyze LCO characteristics present in a flexible model of a wing with freeplay and preloading in its control surface. A wind tunnel test, using a flexible model of a half-wing fitted with a control surface and freeplay, was carried out to verify the results of the developed methodology.

The flexible model was designed to be able to present the nonlinear response known as LCO when installed in the wind tunnel test section and within the operational conditions of the wind tunnel in which the maximum velocity is around $V = 120$ m/s. An important characteristic of this test is that, due to restrictions related to the wind tunnel balance, the model had to be installed on the lateral wall of the test section, generating a condition of preloading on the control surface due to the action of its own weight.

Another characteristic of this test is that, due to the aerodynamic loading, the equilibrium position of the control surface is altered as a function of the flow velocity inside the wind tunnel test section, making it possible to have equilibrium positions inside the freeplay deadspace region. Consequently, it was necessary to adapt specific describing functions for this condition, since the literature, at the time of this wind tunnel test, only treated cases with the equilibrium position outside the freeplay deadspace region.

The results for predictions of control surface equilibrium positions and LCO amplitudes and frequencies were all within an acceptable range and indicate the possibility of using the present describing function and methodology to predict LCO characteristics under freeplay and preloading conditions.

5 REFERENCES

[1] Laurenson, R. M. and Trn, R. M. (1977). Flutter of Control Surfaces with Structural Nonlinearities. Tech. Rep. NASA Report MDC E1734, McDonnell Douglas Astronautics Company.

[2] Worden, K. and Tomlinson, G. R. (2001). *Nonlinearity in Structural Dynamics*. Bristol and Philadelphia: Institute of Physics Publishing. ISBN 0 7503 0356 5.

[3] Verstraelen, E., Dimitriadis, G., Rossetto, G. D. B., et al. (2017). Two-domain and three-domain limit cycles in a typical aeroelastic system with freeplay in pitch. *Journal of Fluids and Structures*, 69, 89–107. ISSN 0889-9746.

[4] Drela, M. (2015). AVL – Aerodynamic Analysis. `http://web.mit.edu/drela/Public/web/avl/`. Accessed: 2015-11-06.

[5] EMBRAER (2015). Aeroelastic Model Freeplay Test Results. Tech. Rep. DT1AAZ004, Embraer S.A.

COPYRIGHT STATEMENT